Climate change impacts on global agricultural land availability

To cite this article: Xiao Zhang and Ximing Cai 2011 *Environ. Res. Lett.* **6** 014014

View the article online for updates and enhancements.

Climate change impacts on global agricultural land availability

Xiao Zhang and Ximing Cai[1]

Ven Te Chow Hydrosystems Laboratory, Department of Civil and Environmental Engineering,
University of Illinois at Urbana-Champaign, Urbana, IL 61801, USA

E-mail: xmcai@illinois.edu

Abstract

Climate change can affect both crop yield and the land area suitable for agriculture. This study provides a spatially explicit estimate of the impact of climate change on worldwide agricultural land availability, considering uncertainty in climate change projections and ambiguity with regard to land classification. Uncertainty in general circulation model (GCM) projections is addressed using data assembled from thirteen GCMs and two representative emission scenarios (A1B and B1 employ CO_2-equivalent greenhouse gas concentrations of 850 and 600 ppmv, respectively; B1 represents a greener economy). Erroneous data and the uncertain nature of land classifications based on multiple indices (i.e. soil properties, land slope, temperature, and humidity) are handled with fuzzy logic modeling. It is found that the total global arable land area is likely to decrease by 0.8–1.7% under scenario A1B and increase by 2.0–4.4% under scenario B1. Regions characterized by relatively high latitudes such as Russia, China and the US may expect an increase of total arable land by 37–67%, 22–36% and 4–17%, respectively, while tropical and sub-tropical regions may suffer different levels of lost arable land. For example, South America may lose 1–21% of its arable land area, Africa 1–18%, Europe 11–17%, and India 2–4%. When considering, in addition, land used for human settlements and natural conservation, the net potential arable land may decrease even further worldwide by the end of the 21st century under both scenarios due to population growth. Regionally, it is likely that both climate change and population growth will cause reductions in arable land in Africa, South America, India and Europe. However, in Russia, China and the US, significant arable land increases may still be possible. Although the magnitudes of the projected changes vary by scenario, the increasing or decreasing trends in arable land area are regionally consistent.

Keywords: climate change, agricultural land, global assessment

S Online supplementary data available from stacks.iop.org/ERL/6/014014/mmedia

1. Introduction

Climate change, resulting from the effects of increased greenhouse gas emissions, poses greater threats than in previous decades by combining higher temperatures, less available water in regions where it is most needed, and more frequent and intense extreme weather events (WFP, FAO, IFRC and OXFAM 2009). In the context of an increasing population,

these effects can become more dramatic. In particular, climate change has raised much concern regarding its impacts on future global agricultural production, varying by region, time, and socio-economic development path (Lobell and Field 2007, Schmidhuber and Tubiello 2007, Schlenker and Lobell 2010). Given the importance of global agriculture, this study examines the impact of climate change on global agricultural land availability, which represents a significant concern for the world's agricultural future, and presents a spatially explicit

---

[1] Author to whom any correspondence should be addressed.

view of the possible global impacts, while considering the uncertainty involved in forecasting future climate change.

Several studies have already explored the global distribution of potential arable land, in terms of biophysical circumstances, under current and future climate conditions (Cramer and Solomon 1993, Xiao 1997, FAO 2000, Ramankutty *et al* 2002). However, in those studies, neither the uncertainty involved in climate change projections nor the ambiguity inherent in land classification (Ahamed *et al* 2000) has been explicitly addressed. Land availability assessments must deal with the challenges involved in land classification according to multiple criteria, and in particular, land assessment at the global scale using international datasets must consider the uncertainty involved in those datasets. Most recently, Cai *et al* (2011) proposed a learning-based, fuzzy logic modeling approach and applied this framework to estimates of global agricultural land availability, represented by probability-based land suitability values. The present study adopts this approach for the land suitability assessment and estimates global agricultural land availability under both current and future conditions.

When considering the uncertainty involved in climate change projections, a systematic approach is needed to treat the various uncertainties associated with model variability and emission scenarios. More than twenty general circulation models (GCMs) have been developed to simulate and predict possible climate changes. Although these models converge acceptably at the global scale, their outcomes at the regional scale vary considerably; some models even conflict with each other (Laurent and Cai 2007). This regional uncertainty arises from two main factors: (1) each model adopts different climate sensitivities (i.e. the temperature change associated with a doubling of the concentration of carbon dioxide in Earth's atmosphere), ranging from 2.1 (PCM) to 4.4 (UKMO-HadGEM1) Celsius (IPCC 2007a, 2007b); and (2) variations between models with respect to combinations of forcings and the quantification methods of common forcings (Collins *et al* 2006, Forster and Taylor 2006, Cai *et al* 2009). Therefore, climate predictions from a single GCM may be insufficient due to limitations within the assumptions, regardless of the model's sophistication. Larger ensemble of GCMs, sampling the widest range of possible outcomes, may provide a more reliable view into the future (Murphy *et al* 2004, Laurent and Cai 2007, Weigel *et al* 2010).

This letter will address several questions related to possible changes in global agricultural land availability given the uncertain projections of climate change.

(a) Do different regions and the world as a whole expect significant changes in agricultural land availability?
(b) What will be the distribution of these possible changes throughout the world?
(c) What is the likelihood of the changes by region?

These questions will be examined by a quantitative land suitability assessment under the various scenarios of projected climate change resulting from the ensemble of thirteen GCMs and two emission scenarios. Regional climate change results are used to derive the changes in land suitability caused by the changes in soil temperature regimes (classified into fourteen categories based on mean annual soil temperature) and humidity. Results are presented for Africa, China, Europe, India, Russia, South America, and the continental United States, all of which are characterized by substantial agricultural production capacities.

2. Data and methodology

2.1. Data processing

Global datasets for land suitability assessment are adopted from Cai *et al* (2011) and provided in table S1 of the supporting information (available at stacks.iop.org/ERL/6/014014/mmedia) (SI, which includes tables S1–6 and figures S1–5, as referred in the rest of this letter is available at stacks.iop.org/ERL/6/014014/mmedia), which includes present soil properties, temperature, humidity index (HI), land slope, and land cover. Specifically, the soil property data used in this work are part of the Harmonized World Soil Database (HWSD) by FAO/IIASA (FAO/IIASA/ISRIC/ISSCAS/JRC 2009) (table S2 available at stacks.iop.org/ERL/6/014014/mmedia). The HWSD contains sixteen soil properties for the earth's land surface, and each property is assigned a rating between 0 and 1. The topographic data used are global terrain slope (GTS) data from Fischer (2008). GTS data include eight slope classes: 0–0.5%, 0.5–2%, 2–5%, 5–10%, 10–15%, 15–30%, 30–45%, and >45%. The slope files contain eight maps, in which the color-coded value of each pixel represents the percentage, by area, belonging to a particular slope class. The land-use data are obtained from the remotely sensed land-cover database from the International Geosphere–Biosphere Program (IGBP) (Biradar *et al* 2009), which serves as a reference for comparison with the simulated results. Each dataset possesses a 30 arcsec resolution.

HI is a numerical indicator of the degree of aridity at a given location and is used in this study as a measure of humidity. A detailed calculation procedure is provided in the SI (available at stacks.iop.org/ERL/6/014014/mmedia). Global HI maps are generated for the historical period and the various projected future scenarios. The generated historical HI map (figure S1 available at stacks.iop.org/ERL/6/014014/mmedia) illustrates similar global patterns to the 1950–2000 global mean HI map generated by Trabucco and Zomer (2009).

It is difficult to simulate the changes in soil temperature regime, which is defined by a number of classes (table S1 available at stacks.iop.org/ERL/6/014014/mmedia) in land classification (Cai *et al* 2011). Since a strong correlation between historical air temperature and soil temperature regimes as defined by USDA-NRCS (USDA-NRCS 1997) is found (see figure S2 available at stacks.iop.org/ERL/6/014014/mmedia), the former is used as a substitute for the latter. Air temperature is divided into three separate ranges: <265 K, 265–280 K, and >280 K, corresponding to the three soil temperature regime classes 3–4, 5–8, and 9–16 (see table S1 for the description, available at stacks.iop.org/ERL/6/014014/mmedia).

Climatic data used in this work contain two periods: (i) historical climatic data, which consist of observed

and simulated thirty-year average monthly land surface temperature and precipitation readings from 1961–1990; and (ii) projected climatic data, consisting of thirty-year average monthly temperature and precipitation forecasts for 2070–2099. Observational historical data are obtained from the Climatic Research Unit (CRU) database at the University of East Anglia (New 1999) and the simulated data are the outputs of thirteen GCMs (CGCM3.1, GFDL-CM2.0, GFDL-CM2.1, GISS-AOM, FGOALS-g1.0, INM-CM3.0, IPSL-CM4, MIROC3.2(hires), MIROC3.2(medres), ECHAM5/MPI-OM, MRI-CGCM2.3.2, CCSM3, UKMO-HadCM3) (IPCC 2007a, 2007b). Since the resolutions of the GCM-simulated outputs vary significantly (from 1.125° by 1.125° to 4° by 5°), all the GCM outputs are re-sampled to 2° by 2° for computational convenience. The observed climate data are also aggregated to the same resolution.

2.2. Uncertainty treatment in regional climate change projections

The regional variability of GCM simulations and the diversity of emission scenarios are considered as the two major sources of uncertainty in climate change projections at the regional scale. Two widely used ensemble approaches are employed to deal with GCM regional variability, the simple average method (SAM) and root mean square error minimization method (RMSEMM). SAM assumes that there is no information available to support the model's preference and assigns an equal weight to each model (Laurent and Cai 2007). This approach ignores the variations in quality between models (Murphy *et al* 2004). RMSEMM determines the weights or skill scores of GCMs according to their relative abilities to reproduce the actual historical records. However, observational datasets usually involve error and uncertainty themselves. Moreover, a model's capacity to reproduce known data is not necessarily representative of its predictive accuracy. These two approaches represent the two extreme cases of information use (Laurent and Cai 2007). These two cases, one rejecting the use of the information from a retrospective analysis and the other fully adopting it, provide very wide, if not the widest, range of the differences among all the combinations of the GCMs used in the study. Given the uncertainty involved in GCM predictions, these two ensemble approaches provide a plausible range of possible future changes. It should be noted that the method adopted in this study uses the ensemble average of the projected climate from a number of GCMs (Murphy *et al* 2004, Weigel *et al* 2010). An optional method is based on scenario screening, i.e., applying individual GCM projections to the land assessment model, which results in a number of land evaluation results (scenarios), and comparing the scenarios to obtain a range of results and a direction or kind of consistency of results. This method may provide useful information regarding the result robustness for individual regions. However, the assumption beyond this scenario screening method is that any single GCM performs properly, and is not inferior to the ensemble of the GCMs. This does not follow the assumption that the ensemble of the GCMs provides better climate prediction than any single GCM

(Murphy *et al* 2004, Weigel *et al* 2010). The debate on the methods is beyond the purpose of this letter. In addition, it is difficult to conduct the scenario screening with a large number of GCMs with land cells of approximately 1 km by 1 km in the global context. Thus the optional method is recommended for a regional study only.

Utilizing SAM, twelve monthly precipitation and temperature files are produced by taking the average of the projected monthly values from thirteen GCMs. In contrast to skill-score-based methods (i.e., applying different weights to individual GCM outputs to calculate weighted average output), RMSEMM is a probability-based method, which targets the optimal performance of the ensemble average of GCM outputs (Laurent and Cai 2007). Probabilities are assigned to each GCM so as to minimize the root mean square error between the 30-year average of the observed historical data and the weighted simulations as shown in following equation.

$$\text{Min } W = \sum_{t=1}^{12} \left(\sum_{i=1}^{13} p_i G_{i,t} - O_t \right)^2; \quad \text{for } t = 1, 2, \ldots, 12,$$
$$i = 1, 2, \ldots, 13.$$

In this case, O_t signifies the monthly observational record, $G_{i,t}$ denotes the monthly simulation of one GCM, p_i represents the probability assigned to a single GCM, and W becomes the annual root mean square error between the weighted simulation and the observation. The probability (p_i) is calculated separately for historical precipitation and temperature (1961–1990) for each grid. Details of this method are provided in Cai *et al* (2011).

In terms of emissions, two scenarios, A1B and B1 are employed to represent a range of emission levels. A1B assumes a future world containing rapid economic growth, low population growth rates, and rapid introduction of more efficient technology. Alternatively, B1 assumes a convergent world with the same global population as in the A1B storyline, but with rapid changes in economic structures, leading toward a more 'green' economy (IPCC 2007a, 2007b). More specifically, A1B projects greater rates of GHG emissions than B1, assuming CO_2-equivalent GHG concentrations of 850 ppmv, compared to 600 ppmv under B1. Thus, A1B is likely to cause temperatures to increase by larger margins by the end of this century. These two scenarios are also chosen because a large sample of GCMs, thirteen in this case, can be assembled under both sets of conditions. Combining the two GCM regional variability treatment methods with the two emission scenarios, four future scenarios are defined and analyzed in this paper: A1B-SAM, A1B-RMSEMM, B1-SAM, and B1-RMSEMM.

2.3. Land classification under future climate conditions

This section follows the methodology developed by Cai *et al* (2011). Land is divided into three categories according to its suitability for agriculture: suitable, marginally suitable, and not suitable. Suitability is characterized by four factors: soil properties, land slope, soil temperature regime, and humidity. FAO proposed two broad land classes, 'suitable' and 'not suitable' based on climatic, terrain and soil property data

(Ahamed *et al* 2000). In this letter, the 'suitable' class defined by FAO is further divided into 'suitable' and 'marginally suitable' classes. Suitable agricultural lands are defined as those locations containing only minor or moderately severe limitations with respect to sustained use. In general, these lands should not contain more than one severe limiting factor among the four factors employed for this assessment (Ahamed *et al* 2000). In reality, these lands will most likely be those currently used as croplands. Marginally suitable lands are those with limitations that are severe in terms of sustained use, but yet marginally economical to cultivate in short term (FAO *et al* 1997). It is assumed that these locations may contain one severe and one moderate limitation or even two moderate limitations, but no more. Marginally suitable lands are most likely to be those currently in use as pasture land, mixed vegetation and cropland, or left fallow. It is also possible that these lands are used primarily as cropland, as may be necessary in certain developing countries. Furthermore, the marginally suitable lands have the potential to be utilized for biofuel crops, such as miscanthus and switchgrass (Tilman *et al* 2009, Cai *et al* 2011). Not suitable lands refer to those sites characterized by more than one severe limitation. In this study, potential arable land is estimated as the sum of suitable lands and marginally suitable lands.

Fuzzy logic modeling is adopted to estimate agricultural land suitability, as it is capable of handling classification uncertainty and ambiguity (Singpurwalla and Booker 2004). It consists of three steps: fuzzification, fuzzy rule inference, and defuzzification (Joss *et al* 2008).

Fuzzification assigns membership functions to each factor for each of the three linguistic variables (suitable, marginally suitable, and not suitable). Next, fuzzy rules are combined and mixed to model the productivity of each land pixel (figure S3 available at stacks.iop.org/ERL/6/014014/mmedia). As an example, the rules for the continental United States are provided in table S3 (available at stacks.iop.org/ERL/6/014014/mmedia). These rules are based upon empirical knowledge and improved through a learning process (table S4 available at stacks.iop.org/ERL/6/014014/mmedia). Finally, defuzzification translates the fuzzy linguistic outputs into an aggregated single value (Oberthur *et al* 2000) (figure S5 available at stacks.iop.org/ERL/6/014014/mmedia). The framework of the integrated land assessment procedures is provided in figure S4 (available at stacks.iop.org/ERL/6/014014/mmedia). One important assumption is that the fuzzy rules which simulate the current arable land will also be able to project the cultivable land in the future. A more detailed description of the approach can be found in the SI (available at stacks.iop.org/ERL/6/014014/mmedia).

Land classification under current climate conditions follows the results from Cai *et al* (2011), which is used as the baseline for the assessment under future climate conditions. The global map of simulated potential arable land under the baseline scenario is displayed in figure S6 (available at stacks.iop.org/ERL/6/014014/mmedia). The baseline land estimates from this study are compared to other studies in tables S5 and S6 in the SI (available at stacks.iop.org/ERL/6/014014/mmedia). Two of the four factors of land suitability,

the HI and soil temperature regimes, are re-assessed using projected changes in precipitation and temperature under the four scenarios defined previously.

3. Results

Global maps of gross potential arable land changes are generated for the four different scenarios: A1B-SAM, A1B-RMSEMM, B1-SAM, and B1-RMSEMM, respectively. Globally, the area of potential arable land ranges from 48.9 (A1B-RMSEMM) to 51.9 (B1-SAM) million km^2, indicating a range of changes [−0.8, 2.2] million km^2 from the baseline estimate of 49.7 million km^2. The arable land total decreases under A1B emission scenarios, but increases under B1. The SAM ensemble approach results in more desirable global outcomes than the RMSEMM, that is, smaller decreases in arable land and larger increases thereof in the analyzed regions. Figures 1(a) and (b) illustrate the distribution of the effects predicted under A1B-RMSEMM and B1-SAM, which represent the largest global arable land decrease and increase, respectively. As can be observed from the two images, arable land is likely to increase at the higher latitudes of the northern and southern hemisphere, including Canada, Russia, northern China, southern Argentina, and the northern US. In comparison, shrinking arability will likely occur at lower latitude locations, such as western Africa, Central America, western Asia, the south-central US, as well as northern and central South America. As shown in table 1, Africa, Europe, India, and South America may expect varying levels of reduction, −1 to −18%, −11 to −17%, −2 to −4%, and −1 to −21% respectively, while Russia, China, and the US may benefit from climate change with increases in arable land of 37 to 67%, 22 to 36% and 4 to 17%, respectively.

The climatic causes of the projected land suitability changes are examined with respect to air temperature and humidity. Figures 2(a) and (b), along with figures 3(a) and (b) display the changes in temperature and HI under the A1B-RMSEMM and B1-SAM forecasts, respectively. Overall, the increases in temperature are milder, and the changes in HI are mostly more favorable to agriculture under B1 as compared with A1B. Regionally, warmer and wetter climate predictions contribute to the increase in cultivable land observed in Russia, northwest China and the northern US. Conversely, a reduction in HI represents the main driver of decreases in cultivable land seen in tropical and sub-tropical areas, affecting crop water availability. Minor decreases in HI are likely to occur in western Asia, southern Europe, Australia, India, the south-central US, and western Africa, while the northern regions of South America may experience slightly more precipitous declines in HI.

When considering suitable land and marginally suitable land separately, both display consistent trends (in terms of gained or lost arable land area) in most regions, with the exception of India. In this case, the suitable potential arable land decreases, while marginally suitable land actually increases in India, indicating an exchange of land between the two categories. By contrast, Russia has some areas which are projected to be converted from marginally suitable to
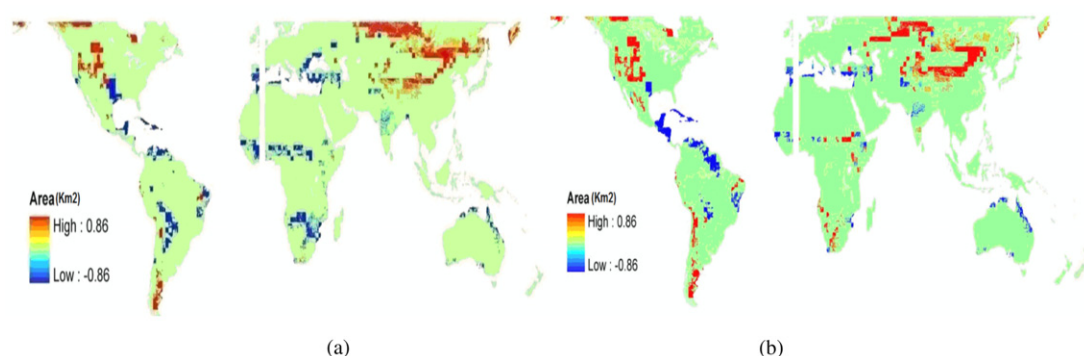
Figure 1. Changes of potential arable land under A1B-RMSEMM (a) and B1-SAM (b). (1) The blank on longitude zero is caused by merging the results from different GCMs with different spatial resolutions, (from 1.125° by 1.125° to 4° by 5°, latitude by longitude); it is also caused by overlaying the GCM results with other spatial datasets (soil, slope and land cover)—the two have different geo-reference systems. During the data converting and aggregation (over different GCM resolutions), some data at the boundary (i.e., longitude zero) are lost. (2) Due to incomplete data in Greenland and Antarctica and the land north of 60 N, these regions are not shown in the map. This notation also applies to figures 2 and 3.
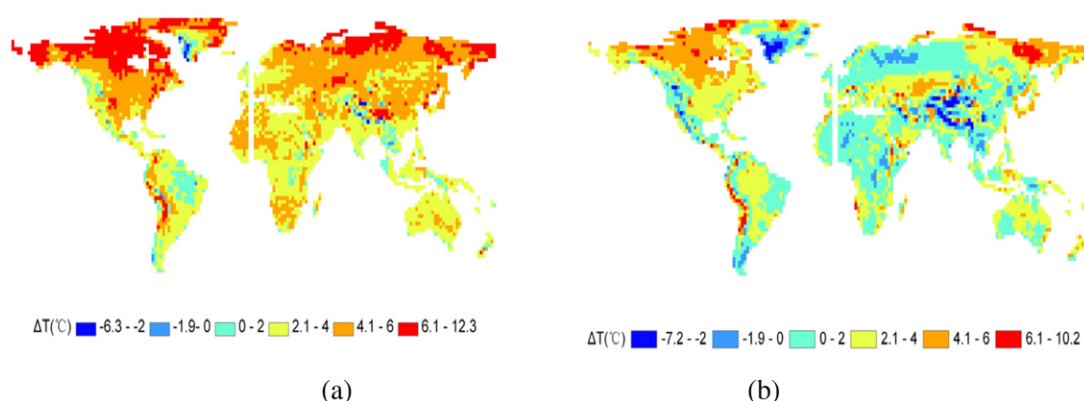

Figure 2. Changes of annual mean temperature under A1B-RMSEMM (a) and B1-SAM (b).

Table 1. Gross potential arable land areas and change percentages under historic and projected scenarios.

	Africa		China		India		Europe		Russia		South America		US		Global	
	Mkm^2	(%)	Mkm^2	(%)	Mkm^2	(%)	Mkm^2	(%)	Mkm^2	(%)	Mkm^2	(%)	Mkm^2	(%)	Mkm^2	(%)
Baseline	12.11		4.58		2.72		3.57		2.32		9.84		4.37		49.74	
A1b-SAM	11.26	−7	6.22	36	2.62	−4	2.97	−17	3.53	52	7.86	−21	4.78	9	49.35	−1
A1b-RMSEMM	9.92	−18	5.71	25	2.64	−3	2.95	−17	3.87	67	8.98	−9	4.53	4	48.92	−2
B1-SAM	12.05	−1	6.03	31	2.67	−2	3.18	−11	3.17	37	9.38	−5	5.11	17	51.91	4
B1-RMSEMM	10.77	−11	5.62	22	2.67	−2	3.17	−11	3.48	50	9.70	−1	4.90	12	50.75	2

suitable land; in northwestern China, some location forecasts even transform from not suitable to suitable land. The forecasted changes in India and Europe depend on the emission scenarios only, while the ranges of conditions projected in the other regions are affected by both the socio-economic development paths (which are associated with the various emission scenarios) and the ensemble approaches. Although the magnitudes of land change vary considerably by scenario, the ordinal directions of change are generally consistent over all scenarios. This indicates that one ought to feel reasonably confident regarding the validity of the obtained arable land availability trends. On the other hand, the ranges of possible

changes do reflect the regional uncertainty associated with the various GCMs as well as their sensitivities to GHG emissions.

In previous studies, the total global potential arable land was estimated, using historical data, as between 32.91 and 41.53 million km^2 (Cramer and Solomon 1993, Xiao 1997, FAO 2000, Ramankutty et al 2002). However, Cramer and Solomon (1993) and Ramankutty et al (2002) did not consider the topography constraint in their estimate, while Xiao (1997) and FAO (2000) adopted 1931–1960 climatic data (Leemans and Cramer 1991), which are colder than the equivalent measurements from 1961–1990 globally (Hadley CRUT 2009). Moreover, the soil property factor adopted
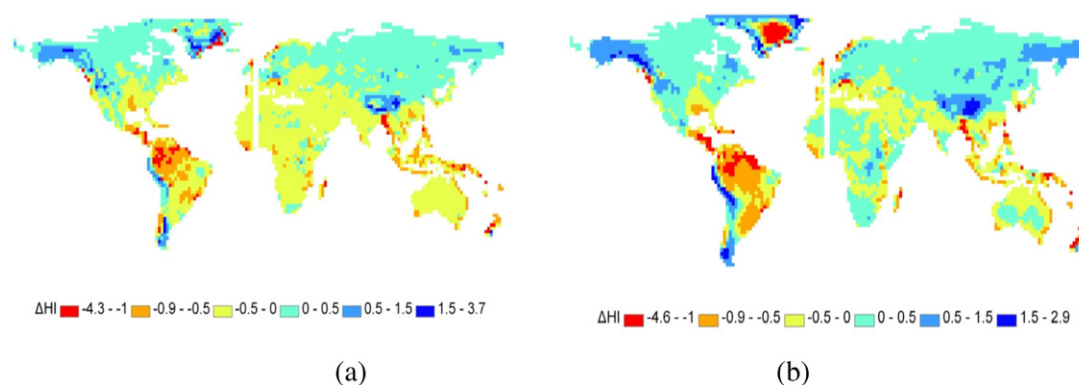
Figure 3. Changes of humidity index under A1B-RMSEMM (a) and B1-SAM (b).

in previous studies (e.g., Cramer and Solomon 1993, Xiao 1997, FAO 2000, Ramankutty *et al* 2002) either has coarser resolution and/or does not include as many properties as this study (table S2 available at stacks.iop.org/ERL/6/014014/mmedia).

When compared with the study by Ramankutty *et al* (2002), for the projected changes in total potential arable land, the regional alteration trends appear consistent while the magnitudes of these shifts do not. Global potential arable land is projected to be reduced by 0.5–0.8 million km^2 under A1B scenarios and increased by 1.0–2.0 million km^2 under the B1 scenarios which represent a greener economy than A1B. To compare, Ramankutty *et al* (2002) predicted an increase of 6.6 million km^2 globally. In general, both this study and another by Collins *et al* (2006) project a reduction in land suitability in tropical regions, such as Africa, South America and Oceania (Ramankutty *et al* 2002) and an increase in regions at the higher latitudes of the northern hemisphere, to varying degrees. Arable land in Russia is predicted to grow by about 1.1 million km^2 in this study; Ramankutty *et al* (2002) estimated an additional 3.4 million km^2 for former Soviet Union. For China, this work projects an increase of around 1.2 million km^2 while Ramankutty *et al* (2002) project 0.9 million km^2 for China, Mongolia and North Korea. In fact, some studies have found that the Inner Mongolia region in China is experiencing rising temperatures and precipitation rates and consequently, should expect grassland expansion as well as improvements in overall yields (e.g., Sheng 2007, You *et al* 2002). The differences may result from the three main reasons besides the different estimating factors employed. First, the various CO_2-equivalent GHG concentration levels are assumed. Ramankutty *et al* (2002) employed the IPCC TAR scenario with a CO_2-equivalent GHG concentrations of 710 ppmv, while this study uses IPCC SRES A1B and B1 scenarios with CO_2-equivalent GHG concentrations of 850 and 600 ppmv, respectively. Second, Ramankutty *et al* (2002) used the anomalies compared to the CRU climatology (i.e., adding the anomalies between the GCM simulations of 2070–2099 and 1961–1990 to the observed 1961–1990 climate data from CRU to eliminate the bias in GCM 2070–2099 simulations, New 1999), while this research adopts GCM projections directly. Third, as discussed above, our study adopts a method based

on the ensemble average climate by two methods (SAM and RMSEMM) and Ramankutty *et al* (2002) basically used the scenario screening method, which applies individual GCM outputs to the land evaluation procedures.

4. Impact of human settlement development

More realistic estimates of land use require adjustments that allow for human settlement in terms of industrial and residential use, as well as for protected land conservation (FAO 2000). A 'protected land' is defined as 'an area of land and/or sea especially dedicated to the protection and maintenance of biological diversity, and of natural and associated cultural resources, and managed through legal or other effective means' (IUCN 1994). This designation includes important forests, woodlands, savannas, grasslands, mountains, lake systems and deserts (Chape *et al* 2003). The breadth of these areas has increased continually, beginning during the middle of the 20th century (Green and Paine 1997). In this study, protected land data from 1994 provided by Green and Paine are adopted for the baseline scenario of climate change assessment. These data are selected due to the temporal proximity of 1994 to the period (1961–1990). It is assumed that the quantity of protected land area in 2003 (Chape *et al* 2003), the most recent year available within the data, would remain constant in the future.

The area required for human settlement is assumed to be related to population size (Alexandratos 1995). In the reference scenario, under current climate conditions, the settlement area is calculated using the conversion of 0.033 ha/person multiplied by the population size. In the projected scenarios, the ratio is slightly less, at 0.03 ha/person, accounting for the assumed higher population density (FAO 2000). The population data used in the reference scenario is from 1992, a year presumed to be similar to the period (1961–1990) used for baseline climate change assessment in this study. The future scenarios employ population data projected for 2050. The selection reflects the fact that the projected world population reaches its peak around 2050 under both A1B and B1 (Furuya *et al* 2009). Furthermore, it was assumed that 50% of the protected areas and 100% of the settlement lands occupy potential arable land (FAO 2000). Based on the specifications stated above, net potential arable land areas are calculated both

Table 2. Net potential arable land areas and change percentages under historic and projected scenarios

	Africa		China		India		Europe		Russia		South America		US		Global	
	Mkm^2	(%)	Mkm^2	(%)	Mkm^2	(%)	Mkm^2	(%)	Mkm^2	(%)	Mkm^2	(%)	Mkm^2	(%)	Mkm^2	(%)
Baseline	10.33		3.79		2.33		3.11		1.96		8.82		3.24		41.32	
A1b-SAM	8.47	−18	5.28	39	2.00	−14	2.45	−21	2.71	38	5.65	−36	3.46	7	38.05	−8
A1b-RMSEMM	7.14	−31	4.77	26	2.02	−13	2.43	−22	3.05	56	6.76	−23	3.20	−1	37.62	−9
B1-SAM	9.26	−10	5.09	34	2.05	−12	2.65	−15	2.35	20	7.16	−19	3.78	17	40.62	−2
B1-RMSEMM	7.99	−23	4.68	24	2.05	−12	2.65	−15	2.66	36	7.48	−15	3.57	10	39.46	−5

worldwide and for seven distinct regions by subtracting the area reserved for protected land and human settlement from the gross arable land present in table 1, and the results are provided in table 2.

The estimated net potential arable land under the baseline scenario is comparable to the current global agricultural area, including cropland and pasture land. According to FAOSTAT (FAOSTAT 2010), the global agricultural area in 1975 is 46.3 million km^2, which exceeds our estimate of 41.3 million km^2. When analyzed by region, the FAO datasets show smaller values for some regions, especially South America. A possible explanation is that a significant fraction of the potential arable land in South America is still undeveloped and covered by forest.

Net arable land around the end of the 21st century under the four scenarios is projected to decline by 2–9% globally. Regionally, Africa, India, Europe and South America are likely to experience different levels of decreased available arable land. By contrast, China, Russia and the US may still benefit from climate change in spite of population growth and land conservation.

5. Discussion and conclusions

Countries at the higher latitudes of the northern hemisphere are more likely to benefit from climate change as a result of increasing quantities of arable land, while countries at medium and low latitudes may suffer from different levels of potential arable land loss. Increases in total potential arable land are likely to occur in regions at the northern hemisphere's higher latitudes, such as Russia, northern China and the US by 37–67%, 22–36%, and 4–17%, respectively. The growth of potential arable land in those regions is mainly attributed to the increased temperature and/or improved humidity, factors which currently constrain land suitability. In Africa and South America, which possess the largest proportions of potential arable land, accounting for more than 40% of the global total, lost arable land can be expected due to climate change by 0.5–18% and 1–21%, respectively. Reductions are also expected in Europe by 11–17% and India by 1.7–3.6%. Globally, the A1B scenarios project a reduction of 0.5–0.8 million km^2 and B1 scenarios project an increase of 1.0–1.2 million km^2. The projected global changes in arable land vary by scenario, which is related to the development paths and GCM ensemble approaches. However, the increasing or decreasing trends in total arable land throughout the different regions is consistent

across all scenarios, allowing for reasonable confidence in the estimates.

The net potential arable land, assessed by subtracting human settlements and protected land from the global total, is estimated as 41.3 million km^2 under the baseline scenario, and is likely to decrease by 0.7–3.7 million km^2 in the projected scenarios. The greatest potential for agricultural expansion lies in Africa and South America, with current cultivated land accounting for less than 20% of the net potential arable land (FAO 2000, Ramankutty *et al* 2002). However, it is likely that both climate change and population growth will cause a reduction in the potential arable land in Africa, South America, India and Europe. Conversely, in Russia, China and the US, although population growth poses a threat to the quantity of arable land, significant increases in net arable land are estimated at 20–56%, 24–39%, and 0–17%, respectively. The increased magnitudes of net arable land in China under the four scenarios are even slightly larger than those of gross arable land. This is probably a result of both climate change impact and slow population growth of China in the future.

This work may overlook possible damages to land quality from extreme events such as heat waves and floods. In some regions, the increasing precipitation rates projected may lead to the expansion of floodplain, and as a result, the reduction of existing croplands; rising sea levels have already caused land losses in certain countries. Moreover, the influences of intra-year climate variability also affect agricultural land use. On the other hand, there are opportunities to increase the value of arable land through adaptive management practices. Some marginally suitable land where water is a constraint may be currently irrigated. It should be noted that more explicit assessment of the impact and limitation and irrigation may result in different arable land, given that irrigation actually supports a large fraction of the world's cropland (Rosegrant *et al* 2002). Other agricultural adaptation measures such as rainfall harvesting and water storage may mitigate the negative impacts of climate change on land suitability and thus maintain current levels of available arable land. These issues suggest a need for more detailed examination at the regional or local scale, but are beyond the scope of this letter.

Although the global scale simulation limits the accuracy of the results required for regional analysis, this letter presents the main patterns and trends of the distribution of potential rain-fed arable land and the possible impacts of climate change from a biophysical perspective, given the data available for our study. The possible gains and losses of arable land in various regions worldwide may generate tremendous impacts

in the upcoming decades upon regional and global agricultural commodity production, demand and trade, as well as on the planning and development of agricultural and engineering infrastructures.

Acknowledgments

References

Ahamed T *et al* 2000 GIS-based fuzzy membership model for crop-land suitability analysis *Agric. Syst.* **63** 75–95

Alexandratos N 1995 *World Agriculture: Towards 2010* (Rome: Food and Agriculture Organization of the United Nations)

Biradar C M *et al* 2009 A global map of rainfed cropland areas (GMRCA) at the end of last millennium using remote sensing *Int. J. Appl. Earth Obs. Geoinf.* **11** 114–29

Cai X *et al* 2009 Assessing the regional variability of GCM simulations *Geophys. Res. Lett.* **36** L02706

Cai X *et al* 2011 Land availability for biofuel production *Environ. Sci. Technol.* **45** 334–9

Chape S *et al* 2003 *2003 United Nations List of Protected Areas* (Gland, Switzerland: IUCN and Cambridge, UK: UNEP-WCMC)

Collins W D *et al* 2006 Radiative forcing by well-mixed greenhouse gases: estimates from climate models in the Intergovernmental Panel on Climate Change (IPCC) fourth assessment report (AR4) *J. Geophys. Res.* **111** D14317

Cramer W P and Solomon A M 1993 Climatic classification and future global redistribution of agricultural land *Clim. Res.* **3** 97–110

FAO 2000 *Land Resource Potential and Constraints at Regional and Country Levels* (Rome: Food and Agriculture Organization of the United Nations)

FAO 1997 Land quality indicators and their use in sustainable agriculture and rural development *Proc. Workshop* (Rome: Food and Agriculture Organization of the United Nations)

FAO/IIASA/ISRIC/ISSCAS/JRC 2009 *Harmonized World Soil Database (Version 1.1)* (Rome: Food and Agriculture Organization of the United Nations and Laxenburg, Austria: IIASA)

FAOSTAT 2010 Land statistics, ResourceSTAT (Rome: Food and Agriculture Organization of United Nations)

Fischer G E A *et al* 2008 *Global Agro-Ecological Zones Assessment for Agriculture (GAEZ 2008)* (Laxenburg, Austria: IIASA and Rome: Food and Agriculture Organization of United Nations)

Forster P and Taylor K E 2006 Climate forcings and climate sensitivities diagnosed from coupled climate model integrations *J. Clim.* **19** 6181–94

Furuya J *et al* 2009 Impacts of global warming on the world food market according to SRES scenarios *World Academy of Science, Engineering and Technology* **57** 24–29

Green M J B and Paine J 1997 State of the world's protected areas at the end of the twentieth century *INCN World Commission on Protected Areas Symposium (Albany, Australia, 24–9 November 1997)* (Cambridge, UK: World Conservation Monitoring Centre)

Hadley CRUT 2009

IPCC 2007a *IPCC Fourth Assessment Report: Climate Change 2007: Working Group I: The Physical Science Basis* (Cambridge, UK: Cambridge University Press)

IPCC 2007b *IPCC Fourth Assessment Report: Working Group III: Mitigation of Climate Change* (Cambridge, UK: Cambridge University Press)

IUCN 1994 *1993 United Nations List of National Parks and Protected Areas* (Gland, Switzerland: IUCN and Cambridge, UK: UNEP-WCMC)

Joss B N *et al* 2008 Fuzzy-logic modeling of land suitability for hybrid poplar across the Prairie Provinces of Canada *Environ. Monit. Assess.* **141** 79–96

Laurent R and Cai X M 2007 A maximum entropy method for combining AOGCMs for regional intra-year climate change assessment *Clim. Change* **82** 411–35

Leemans R and Cramer W 1991 The IIASA database for mean monthly values of temperature, precipitation and cloudiness of a global terrestrial grid (Laxenburg, Austria: IIASA)

Lobell D B and Field C B 2007 Global scale climate-crop yield relationships and the impacts of recent warming *Environ. Res. Lett.* **2** 014002

Murphy J M *et al* 2004 Quantification of modelling uncertainties in a large ensemble of climate change simulations *Nature* **430** 772

New M E A 1999 Representing twentieth century space-time climate variability. Part 1: development of a 1961–90 mean monthly terrestrial climatology *J. Clim.* **12** 829–56

Oberthur T *et al* 2000 Using auxiliary information to adjust fuzzy membership functions for improved mapping of soil qualities *Int. J. Geogr. Inf. Sci.* **14** 431–54

Rosegrant M *et al* 2002 *World Water and Food to 2025: Dealing with Scarcity* (Washington, DC: Int'l Food Policy Research Institute)

Ramankutty N *et al* 2002 The global distribution of cultivable lands: current patterns and sensitivity to possible climate change *Global Ecol. Biogeogr.* **11** 377–92

Schlenker W and Lobell D B 2010 Robust negative impacts of climate change on African agriculture *Environ. Res. Lett.* **5** 014010

Schmidhuber J and Tubiello F N 2007 Global food security under climate change *Proc. Natl Acad. Sci.* **104** 19703–08

Sheng W 2007 *Simulation of Climate Change Impacts on the Ecological System in Inner Mongolia* (Beijing: Chinese Academy of Agricultural Sciences)

Singpurwalla N D and Booker J M 2004 Membership functions and probability measures of fuzzy sets *J. Am. Stat. Assoc.* **99** 867–77

Tilman D *et al* 2009 Beneficial biofuels-the food, energy, and environment trilemma *Science* **325** 270–71

Trabucco A and Zomer R J 2009 Global Aridity Index (Global-Aridity) and Global Potential Evapo-Transpiration (Global-PET) Geospatial Database (Washington, DC: CGIAR Consortium for Spatial Information)

USDA-NRCS 1997 Soil Climate Map, Soil Survey Division (Washington, DC: World Soil Resources)

Weigel A P *et al* 2010 Risks of model weighting in multimodel climate projections *J. Clim.* **23** 4175–91

WFP, FAO, IFRC and OXFAM 2009 Climate change, food insecurity and hunger *(Technical Paper for the IASC Task Force on Climate Change)*

Xiao X 1997 Transient climate change and potential croplands of the world in the 21st century *Report #18* (Cambridge, MA: Massachusetts Institute of Technology)

You L *et al* 2002 Climate change of Inner Mongolia in the near 50 years and prospects in the next 10–20 years *Meteorol. J. Inner Mongolia* **4** 467